Jordan Journal of Civil Engineering, Volume **19**, No. **1**, **2025**
DOI: https://doi.org/10.14525/JJCE.v19i1.07

Jordan Journal of Civil Engineering

Journal homepage: https://jjce.just.edu.jo

Numerical Study of Supercritical Flow over Mesh-panel Bottom Rack Used to Estimate the Dividing Discharge Streamline in Clear Water Conditions

Keivan Bina [1)*], ***Shahab RikhtehgarMashhad*** [2)], ***Mahdi Behnamnik*** [3)]

[1)] *Assistant Professor, Department of Civil Engineering, Faculty of Engineering, Khayyam University, Mashhad, Iran.*
** Correspondence Author. E-Mail: k.bina@khayyam.ac.ir*
[2)] *Graduated Master in Civil Engineering, Faculty of Civil Engineering, Semnan University, Semnan, Iran.*
E-Mail: shahab.rm1987@gmail.com
[3)] *Graduated Master in Civil Engineering, Hydraulic Structures, Islamic Azad University (IAU), Mashhad, Iran.*
E-Mail: behnamnik-m@mashhad.ir

ARTICLE INFO

Article History:
Received: 5/7/2024
Accepted: 17/12/2024

ABSTRACT

Bottom racks are critical for diverting flow for small hydropower projects. This study investigates the hydraulic behavior of a mesh-panel bottom rack, comprising longitudinal and transverse bars, under clear-water conditions using a numerical model developed with the Flow-3D finite volume code. The research focuses on the discharge dividing streamline (DDS) and derives an empirical regression equation for its position based on model results. The numerical model is calibrated and validated against experimental data from Bina and Saghi (2017), yielding average relative errors of 3.4% for diverted discharge (Qd) and 1.9% for remaining discharge (Qr). The pressure distribution and vertical flow velocity analyses reveal that negative pressure around the transverse bars enhances diverted discharge. The vertical velocity distribution shows that outflow begins after approximately 30% of the rack length. The deep velocity distribution extracted from the Flow-3D model matches experimental data well, achieving a coefficient of determination (R^2 = 0.98) and a relative error (Er = 0.32%). This study proposes a regression relation to estimate the normalized DDS position, facilitating easy determination of diverted discharge in river diversion projects by measuring the approaching flow depth.

Keywords: Bottom rack, Diverted discharge ratio (DDR), Discharge dividing streamline (DDS), Flow-3D numerical model, Hydraulic behavior, Vertical flow velocity.

INTRODUCTION

Bottom intakes are structures placed in the riverbed to divert a portion of the flow to a canal underneath the riverbed. This study builds on the foundational work of bottom rack intake systems, incorporating insights from recent advances in hydraulic engineering and environmental hydraulics. According to Novak and Nalluri (2001), hydraulic structures play a crucial role in managing water resources effectively. Additionally, Chanson (2004) emphasized the importance of environmental considerations in open channel flow design. This low-cost structure is a key element of hydropower systems, especially useful in mountainous rivers with steep slopes (Andaroodi, 2005). Some advantages of these structures compared with other diverting structures include preventing upstream sedimentation and avoiding changes in the topography of the watershed. Sediment transport and its effects on hydraulic structures have been extensively explored by Guo and Julien (2008). Their modified log-wake law provides a more accurate prediction of flow characteristics in open-channel flows, which is critical for designing efficient bottom rack systems. The structures are also extremely stable, cost-effective, and not seasonal (Andaroodi, 2005; Bina & Saghi, 2017). While the primary focus of this study is on hydraulic efficiency, it is essential to consider the environmental impacts of such structures. Ecological implications are among the most important issues related to the exploitation of bottom intakes. Such structures have less ecological impacts than the construction of a diversion dam structure in rivers, because they do not prevent the accumulation of sediments in the upstream side, do not prevent fish from passing through the river section, and generally have less impact on changing the river topography and the natural habitat of aquatic animals, pollutant retention upstream of the weir, habitat fragmentation and heterogeneity reduction in the de-watered river reach (Alban Kuriqi et al., 2021), but their adverse ecological effects should still be investigated. Chanson (2004) and O'Hara and Pelletier (2007) highlighted the importance of designing hydraulic structures that facilitate fish passage and minimize habitat disruption. For example, clogging of the screen of these structures due to bed-load sediment should be controlled by optimal designing of the rack geometric parameters in proportion to the grain size of the river bed load. To do this, the screen installation slope and the free distance between the bars (rack clearance) can be designed in such a way that causes the sediment to slip and pass, preventing the rack from clogging or preventing fish from being trapped or injured. It should be noted that such structures are suitable for mountainous rivers with coarse bed load and high slopes.

Significant research has been conducted to adjust the diverted discharge coefficient (DDC) by utilizing longitudinal or transversal bars (Righetti & Lanzoni, 2008; Bina & Saghi, 2017; Castillo et al., 2017). Since Orth et al. (1954) presented the first hydraulic description of the bottom rack intake, various researchers have focused on estimating the DDC of bottom racks as a main practical design parameter (Castillo & Delgado, 2015; Orth et al., 1954; Guo & Julien 1997; Julien & Simons, 1985; Chanson, 2004; Guo, 2002; Novak et al., 2001; Hager, 2010). Others have studied the rack's hydraulic performance using physical or numerical modeling (Henderson, 1966; Righetti & Lanzoni, 2008; Noseda, 1956; Brunella et al., 2003). The diverted discharge across the bottom intake can be obtained by solving Equation (1):

$$-\frac{dQ}{dx} = C_d .\varepsilon.B.\sqrt{2gY} \tag{1}$$

where Y is the hydraulic head, g is the gravitational constant, B is the rack width, Cd is the DDC, and ϵ is the rack void ratio (Kumar et al., 2010). The discharge coefficient (Cd) and hydraulic head (Y) vary based on rack geometry, bar shapes, and the hydraulic characteristics of the approaching flow (Castillo et al., 2013). One main objective of studying bottom racks under different conditions is to estimate the diverted discharge flow. Bina (2018) used an empirical equation to estimate the discharge diverted by the bottom intake, utilizing the Discharge Dividing Streamline (DDS) rather than Equation (1) (Bina, 2018). When the streamlines that cross the bottom racks are drawn, a single streamline ends at the rack's downstream, as shown in Figure (1). This streamline, called the Discharge Dividing Streamline, separates the streamlines redirected by the bottom rack (Qd) from those that pass through the rack (Qr), as depicted in Figure (1).

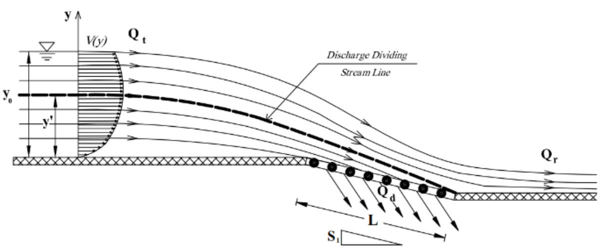

Figure (1): Schematic representation of the discharge dividing streamline position over the bottom rack (Bina, 2018)

Understanding the height of the DDS on the upstream side of the bottom rack (y′) over the channel bed helps estimate the discharge rate of the diverted flow. The equation of deep flow velocity distribution on the upstream side of the bottom rack is given by Eq. (2):

$$Q_d = \int_0^{y'} BV(y)dy \tag{2}$$

where Qd is the diverted discharge flow by the bottom rack, B is the rack width, V(y) is the deep velocity distribution function in the upstream channel section, and y′ is the position of the DDS compared with the channel bed. Using Buckingham's theory and regression, Bina defined an empirical formula to estimate the location of the DDS based on a series of laboratory tests. He proposed a new bottom rack design, the "Mesh-panel bottom rack" (Bina & Saghi, 2017, Bina, 2018). Bina's design includes longitudinal bars along the stream at the top layer and transverse bars at the bottom layer. The longitudinal bars increase the diverting flow and reduce sediment clogging, while the transverse bars support and anchor the longitudinal bars against heavy mountain river rocks (Bina, 2018). Calibrated mathematical models can eliminate the need for physical experimentation, which is costly, time-consuming, and requires measurement instrumentation. In this analysis, the numeric model is based on the physical models built and tested by Bina to investigate stress and vertical flow velocity across the rack and, above all, to estimate the normalized DDS location.

EXPERIMENTAL MODEL

Bina and Saghi (2017) and Bina (2018) experimentally studied the flow passing through racks in the mesh-panel bottom intake. Their research focused on both geometrical parameters (rack length and slope) and hydraulic parameters (discharge and Froude number). They measured discharges (diverted by the intake and passing over the intake) and velocity using a calibrated miniature propeller apparatus and two sharp-crested, fully aerated rectangular weirs (Patil et al., 2021; Saleh & Khassaf, 2023); The flume characteristics and its equipment are illustrated in Figure (2). The study was carried out in a flume 8 meters long and 40 centimeters wide with clear plexiglas sidewalls (Khodier & Tullis, 2022). The mesh-panel bottom racks with different lengths, the same width, and circular cross-section bars were built and placed on the channel bed. In each experimental run, different approach flows passed over the bottom rack and divided into two parts: one diverted flow to the downstream lower apron (Qd) and the other flow passed over the rack and remained in the downstream upper apron (Qr). A two-story channel structure with a steel frame and clear plexiglas sidewalls, equipped with two sharp-crested, fully aerated, calibrated rectangular weirs, was constructed to measure Qd and Qr separately and attached to the end of the main flume (See Figures 2-6).

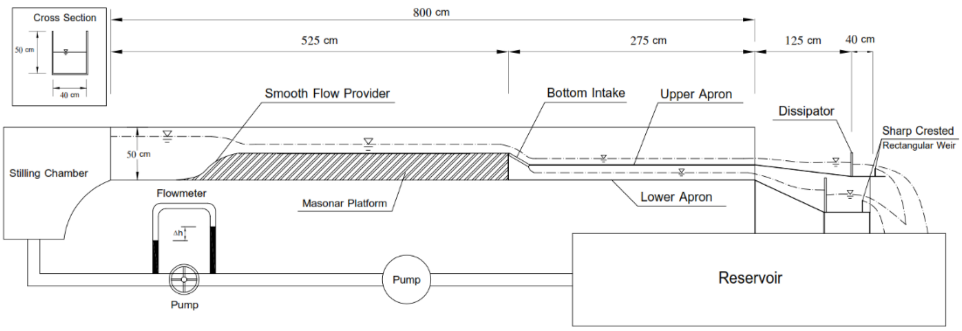

Figure (2): Sketch of the experimental setup components (Bina & Saghi, 2017)

Figure (3): Experimental setup: a) left picture, setup overview,
b) right picture, mesh-panel bottom rack, downstream view (Bina & Saghi, 2017)

Figure (4): The upper and lower apron and rack position in experimental setup before and during run (Bina & Saghi, 2017)

Figure (5): The upper and lower apron along flume from different views and the position of the two-story measuring channel (Bina & Saghi, 2017)

Figure (6): The two-story measuring channel attached to the end of main flume and equipped with two sharp crested rectangular weirs (Bina & Saghi, 2017)

Test parameters for non-sediment flow conditions used in this study are summarized in Table 1. Bina and Saghi (2017) performed 81 tests in clear-water conditions for 3 void ratio values of mesh-panel bottom rack (0.3, 0.35 and 0.4). The numerical model of the current study was built based on a single bottom rack void ration of 0.4 (see Table 1), So, only 27 out of 81 test series of Bina and Saghi (2017) that relate to the void ratio of 0.4 were used in this study. The test data from Bina's work, which is used for validation of the numerical model, is presented in Table 2.

Table 1. Test parameters in clear water conditions from Bina's work (Bina & Saghi, 2017)

Parameters	Notation	Values
Rack slope (%)	S_1	22-57
Rack void ratio (%)	ε	40
Rack length (cm)	L	15-30
Test discharge (l/s)	Q_t	10-30
Froud Number	Fr	>1

Table 2. Experimental data for flow over the mesh-panel from Bina's work (Bina, 2018) used to validate the numerical model in this study

Test No.	L (mm)	S_1 %	ε	Fr_0	Q_T (l/s)	Q_r (l/s)	Q_d (l/s)
T60	299	56.98	0.40	1.56	11.48	0.30	11.18
T61	154	56.30	0.40	1.56	11.48	1.22	10.31
T62	234	57.35	0.40	1.56	11.48	0.52	10.87
T63	299	56.98	0.40	1.58	19.82	2.95	16.79
T64	154	56.30	0.40	1.58	19.82	7.55	12.34
T65	234	57.35	0.40	1.58	19.82	3.90	15.79
T66	299	56.98	0.40	1.54	29.12	8.60	19.56
T67	154	56.30	0.40	1.54	29.12	13.77	15.35
T68	234	57.35	0.40	1.54	29.12	9.42	18.85
T100	299	27.24	0.40	1.57	12.62	0.12	12.34
T101	152	27.70	0.40	1.57	12.62	0.26	12.04
T102	234	28.19	0.40	1.57	12.62	0.06	12.34
T103	299	27.24	0.40	1.60	21.32	0.96	19.92
T104	152	27.70	0.40	1.60	21.32	4.51	16.12
T105	234	28.19	0.40	1.60	21.32	1.09	19.56
T106	299	27.24	0.40	1.51	32.93	3.70	28.85
T107	152	27.70	0.40	1.51	32.93	13.93	17.98
T108	234	28.19	0.40	1.51	32.93	6.31	25.60
T230	299	21.16	0.40	1.56	10.45	0.00	10.45
T231	153	21.16	0.40	1.56	10.45	0.06	10.31
T232	234	21.16	0.40	1.56	10.45	0.00	10.45
T233	299	21.16	0.40	1.58	20.35	0.73	19.56
T234	153	21.19	0.40	1.58	20.35	3.90	16.45
T235	234	22.17	0.40	1.58	20.35	0.84	19.21
T236	299	21.16	0.40	1.53	32.68	2.09	30.54
T237	153	21.19	0.40	1.53	32.68	11.14	20.65
T238	234	22.17	0.40	1.53	32.68	4.73	27.21

In the above table, L is the rack length, S1 is the rack slope, ε is the rack void ratio, Fr0 is the upstream approaching Froude number, Qt is the total upstream discharge, Qd is the diverted discharge by the bottom rack, and Qr is the discharge passed over the rack.

In recent years, attempts have been made to tackle the air-water flow in hydraulic structure problems using Computational Fluid Dynamics (CFD) models (Bina et al., 2024; Castillo et al., 2016; Wong, 2010). With the Volume-of-Fluid (VoF) method, the interface between water and air can be located and tracked as it moves through the computational domain. For bottom rack intakes, Wong (2010) attempted a CFD simulation on a supercritical bottom rack chamber using Flow-3D; however, due to coarse grid resolution, details of the rack interception could not be resolved with high accuracy. Castillo and Delgado (2015) used the VoF method to simulate flow from a sub-critical bottom rack and validated their model by comparing numerical results with experimental data.

NUMERICAL MODEL

Model Geometry

In our computational fluid dynamics (CFD) simulations, we adopted methods outlined by Anderson (1995) and Ferziger and Peric (2002) to enhance the accuracy and reliability of our models. The simulation domain's geometry is shown in Figure (7). To reduce computational time, three mesh blocks with different mesh sizes were used in various zones of the simulation domain. The first mesh block was located at the upstream canal before the intake, with a length of 350 cm and a mesh size of 8 mm to ensure uniform and fully developed flow. The second mesh block, the intermediate or bottom intake block, had varied lengths and a 4-mm mesh size to enhance the precision of bars and clearance modeling. The final block is a downstream channel block after the intake, with a length of 40 cm and a mesh size of 8 mm. Figure (7) shows the block locations, and Table 3 lists the mesh properties after performing mesh sensitivity analysis.

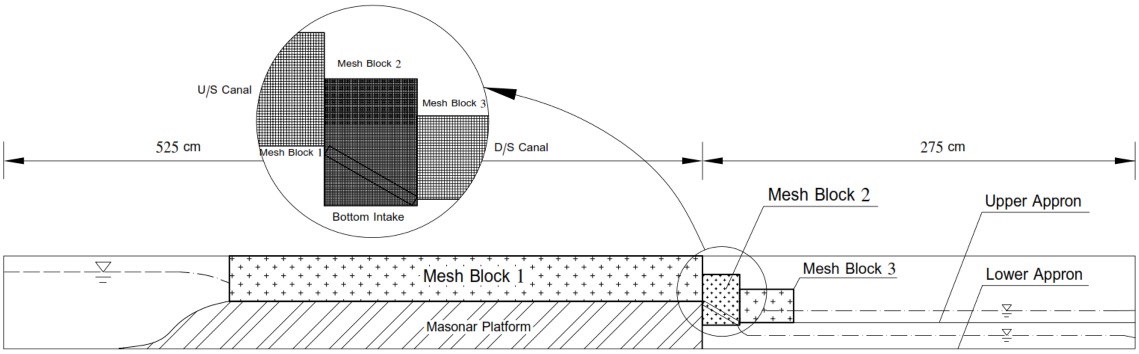

Figure (7): Longitudinal profile of the canal and the bottom rack in the model with three mesh blocks

Table 3. Mesh blocks and cell numbers

Mesh Block	Block Position	Mesh size (m)	Number of Cells
1	Upstream Canal	0.004	394400
2	Mesh-panel Intake	0.002	206250
3	Downstream Canal	0.004	10400

In this simulation, water was considered with a flow viscosity of 0.001 m²/s, a density of 1000 kg/m³, a surface tension of 0.073 kN/m, gravity acceleration of 9.81 m/s², atmospheric pressure of 1.013×10^5 Pa, and a room temperature of 20 °C (Novak et al., 2001).

Governing Equations

Flow-3D was used to solve Navier-Stokes equations within a defined control volume. The continuity and momentum Navier-Stokes equations for incompressible flow are shown below (Eqs. (3) & (4)).

$$\frac{\partial u_i}{\partial x_i} = 0 \tag{3}$$

$$\frac{\partial}{\partial x_i}(u_i u_j) = -\frac{\partial p}{\partial x_i} + \frac{\partial \tau_{ij}}{\partial x_j} g \tag{4}$$

where i and j are standard tensor notations, u_i is the time-averaged velocity component in the x direction, p is pressure, g is gravity acceleration, ρ is density, and τ_{ij} is a stress tensor which can be written as in Equation (5):

$$\tau_{ij} = \left[\rho(\nu + \nu_t)\left[\frac{\partial u_i}{\partial x_j} + \frac{\partial u_j}{\partial x_i}\right]\right] - [\frac{2}{3}\rho(k_T + \vartheta_t)\frac{\partial u_i}{\partial x_i}\delta_{ij}] \tag{5}$$

ν and ν_t represent the kinematic viscosity of the fluid and the viscosity of turbulence, respectively, k_T is the turbulence kinetic energy, and δ_{ij} is the Kronecker delta. Different turbulence models are used in this study.

Boundary Conditions

Boundary conditions are crucial in computational fluid dynamics. In this study, boundary conditions include a flow inlet, flow outlet, rigid boundary, and the boundary of the water surface. The flow volume rate is defined for an inlet with a specified water surface elevation and discharge. An outflow boundary is used at the outlets, as the details of flow velocity and pressure are unknown prior to solving the flow problem (Ghasemzadeh, 2013; Bina et al., 2024). A rigid boundary is defined using a standard wall function. A symmetrical boundary condition is applied to the middle block and water surface. Figure (8) illustrates the boundary conditions for all mesh blocks in two dimensions and the intermediate mesh block in three dimensions. Table 4 lists the boundary conditions for all mesh blocks in the current study.

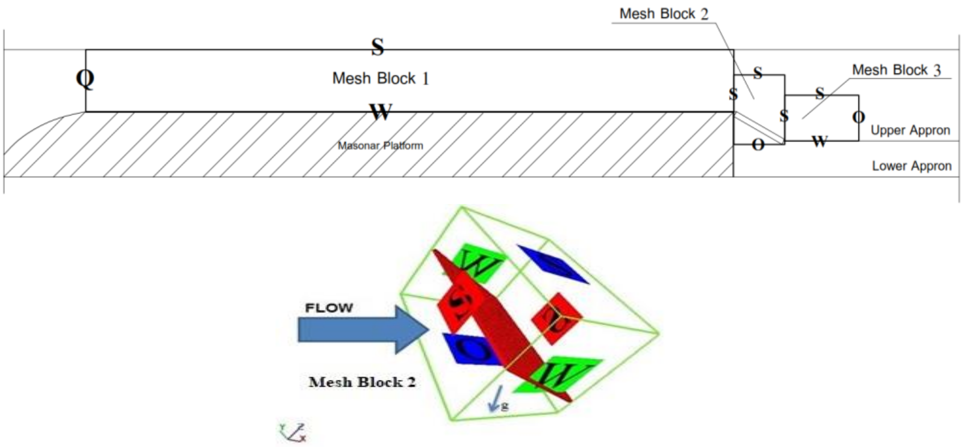

Figure (8): Boundary conditions for the mesh block containing the bottom rack, including the wall condition (W), the symmetry condition (S), and the outflow condition (O)

Table 4. Boundary conditions for all mesh blocks

z-down	z-up	y-left	y-right	x-downstream	x-upstream	Block Position	Block No.
W	S	W	W	S	(Q) Volume Flow rate	upstream canal	1
O	S	W	W	S	S	intermediate block	2
W	S	W	W	O	S	downstream canal	3

Time Step

The time step can be automatically calculated by Flow-3D or entered by the user. The time step can change automatically, provided stabilization conditions are not violated. In this simulation, the time step is selected as 1% of total time. If this value creates an unstable solution, the time step will be reduced by 50%, and parameters will be recalculated until stability conditions are met. If a stable solution is established at 1%, the time step will be increased by 50% to achieve a fast and stable solution. The total time for each simulation averaged 60 seconds, with the time step automatically set at 0.6 seconds.

Turbulence Model

Due to the different behavior of turbulence models in complex flow conditions around the bottom intake, the influence of the turbulence model was tested with five models: The Prandtl mixing length model, the single equation model, the standard k-ε model, the RNG k-ε model, and the large Eddy simulation (LES) model. To determine the best turbulence model for this simulation and calibration of the numerical model, the values of the numerical diverted discharge (Qd) from the

FLOW-3D model using different turbulence models were compared with experimental values of Qd for three tests (T61, T64, and T67). The selection of tests T61, T64, and T67 was made due to their ability to reflect varying flow conditions and their relevance to the study objectives. These three tests covered the whole range of discharge values from 11.48 l/s to 29.12 l/s. Test T61 simulated a moderate flow discharge (QT=11.48 l/s) with a Froude number (Fr=1.56), resulting in a diverted discharge (Qd=10.31 l/s) and a remaining discharge (Qr=1.22 l/s). This test represents a typical supercritical flow condition with moderate discharge values. Test T64 examined higher flow discharge conditions (QT=19.82 l/s) and a Froude number (Fr=1.58), yielding a diverted discharge (Qd=12.34 l/s) and a remaining discharge (Qr=7.55 l/s), making it suitable for evaluating the model's performance under higher flow conditions. Test T67 simulated the highest flow discharge (QT=29.12 l/s) with a Froude number (Fr=1.54), producing a diverted discharge (Qd=15.35 l/s) and a remaining discharge (Qr=13.77 l/s). The performance of each turbulence model was evaluated by comparing Qd predictions from numerical simulations with experimental data. The estimation errors of Qd were calculated and compared in terms of the coefficient of determination (R^2), the Root Mean Square Error (RMSE), and the Mean Absolute Error (MAE), as recommended by Hosseini et al. (2015). The closer the MAE and RMSE values are to zero, the better the model matches the experiment. As shown in Table 5, the difference between diverted discharge calculated by the RNG k-ε model and the experimental data was the smallest, making it the most suitable model for this study. Researchers who previously modeled similar conditions also suggested using the RNG k-ε turbulence model (Hosseini et al., 2015; Ghaderi et al., 2020; Bina et al., 2024).

Table 5. Evaluation of turbulence models

Turbulence model	R^2	RMSE (l/s)	MAE (l/s)
Single equation	0.9	0.8	0.82
k-ε Standard	0.95	0.43	0.54
RNG k-ε	0.98	0.01	0.05
Prandtl mixing length	0.87	1.42	1.06
Large eddy simulation	0.83	1.54	1.24

Model Assessment

Validation was carried out by comparing experimental and numerical simulations on discharge diverted flow by the bottom intake (Qd) and discharge passed over the bottom intake (Qr). Results for the 24 tests with different discharges are presented in Table 6 and Figure (9), comparing Qd for experimental and numerical results. The relative error (Er) of estimating Qd was calculated using Equation (6):

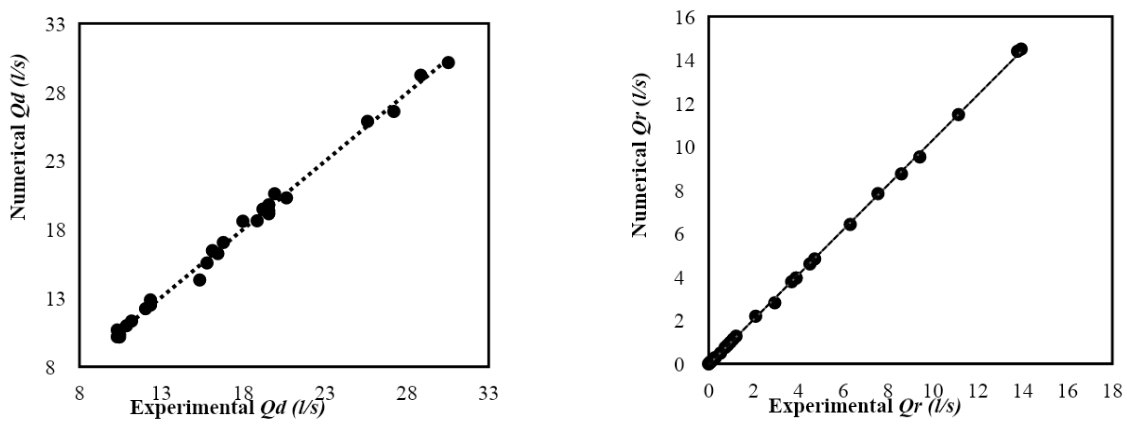

Figure (9): Comparison of numerical and experimental results for flow discharges over the bottom intake, a) for Qr and b) for Qd in all tests

Table 6. Summary of model results for Q_d and Q_r and estimation errors

Test No.	Boundary Conditions				Model Results		Error (%)	
	Q_T (l/S)	Y_0 (mm)	Q_r (l/s)	Q_d (l/s)	Q_r (l/s)	Q_d (l/s)	Q_r	Q_d
T60	11.48	33	0.30	11.18	0.28	11.33	5.76	-1.31
T61	11.53	33	1.22	10.31	1.27	10.68	-4.34	-3.61
T62	11.39	33	0.52	10.87	0.49	10.99	6.08	-1.07
T63	19.73	47	2.95	16.79	2.81	17.05	4.6	-1.56
T64	19.88	47	7.55	12.34	7.84	12.48	-3.87	-1.17
T65	19.69	47	3.90	15.79	3.95	15.56	-1.37	1.46
T66	28.16	62	8.60	19.56	8.75	19.34	-1.8	1.14
T67	29.12	62	13.77	15.35	14.4	14.32	-4.56	6.68
T68	28.27	62	9.42	18.85	9.53	18.63	-1.22	1.19
T100	12.45	35	0.12	12.34	0.12	12.49	-0.82	-1.25
T101	12.29	35	0.26	12.04	0.27	12.23	-5.15	-1.6
T102	12.40	35	0.06	12.34	0.066	12.54	-2	-1.66
T103	20.89	49	0.96	19.92	0.99	20.6	-2.76	-3.4
T104	20.63	49	4.51	16.12	4.6	16.46	-1.94	-2.1
T105	20.65	49	1.09	19.56	1.13	19.79	-3.89	-1.16
T106	32.55	68	3.70	28.85	3.78	29.23	-2.2	-1.31
T107	31.92	68	13.93	17.98	14.5	18.6	-4.06	-3.43
T108	31.91	68	6.31	25.60	6.42	25.87	-1.71	-1.06
T230	10.45	31	0.00	10.45	0	10.17	0	2.66
T231	10.37	31	0.06	10.31	0.07	10.18	-8.18	1.24
T232	10.45	31	0.00	10.45	0	10.34	0	1.04
T233	20.29	48	0.73	19.56	0.75	19.14	-2.6	2.17
T234	20.35	48	3.90	16.45	3.95	16.24	-1.37	1.3
T235	20.05	48	0.84	19.21	0.86	19.48	-1.84	-1.42
T236	32.63	67	2.09	30.54	2.19	30.15	-4.57	1.27
T237	31.79	67	11.14	20.65	11.48	20.3	-3.06	1.68
T238	31.93	67	4.73	27.21	4.83	26.59	-2.22	2.26

$$E_r = \frac{(Q_d)_a - (Q_d)_c}{(Q_d)_a} \times 100 \tag{6}$$

where (Qd)a is the measured Qd from Bina's (Bina, 2018) work, and (Qd)c is the numerical Qd from the Flow-3D model. The relative error (Er) for Qs was calculated similarly. The average relative errors for Qd and Qs were 3.4% and 1.9%, with standard deviations of 5.41% and 8.25%, respectively. This indicates appropriate coordination between experimental and model results, confirming the numerical model's accuracy and its applicability to various flow conditions.

It can be seen from Table 6 that:

- 6 out of 27 tests (22% of tests) in Table 5 have discharge (Qd or Qr) estimation errors between 4% and 5%.
- 2 out of 27 tests (7.4% of tests) in Table 5 have discharge (Qd or Qr) estimation errors between 5% and 6%.
- 19 out of 27 tests (70% of tests) in Table 5 have discharge (Qd or Qr) estimation errors of less than 4%, which is desirable.
- For the tests with more than 4% error in discharge estimation (8 cases), just one case (T67) was related to the error in Qd estimation, and the rest were related to the error in Qr estimation.
- For the tests with more than 4% error in discharge

estimation (8 cases), just two cases were related to the maximum total discharge (QT) of 30 l/s, one case was related to the medium total discharge of 20 l/s, and five cases were related to the minimum total discharge of 10 l/s -12 l/s.

Upon further examination of the results and the experimental process, it was determined that the error in laboratory measurements of flow at minimum flow rates related to the low height of the flow over the sharp-crested rectangular weir (Hd), in the upper portion of the flow measurement channel (see Fig. (2) and Fig. (6)). When the flow height is less than 2 cm, the adhesion of the lower nappe to the downstream body of the weir can influence the height of the passing flow height. Consequently, this affects the accuracy of the remaining discharge (Qr) measurements.

Also, in maximum total discharge (QT) of 30 l/s, the accuracy of water height readings in both the upper and lower channels was high due to turbulence and fluctuations in the water level, resulting in increased errors in both discharge measurements (Qd and Qr).

It is important to note that all experiments with discharge measurement errors exceeding 4% were conducted multiple times. Secondly, in this study, the height of the DDS (y′) was estimated using experimental parameters (Table1), and the discharge values (Qd or Qr) were not used. Additionally, the results from experiments with discharge errors greater than 4% were not included in the validation of the numerical model.

Mesh Independency

Using multi-block meshing technique and adjusting mesh sizes in different regions improved the accuracy of simulations and provided more reliable results. This focus on mesh sizes offers optimized and reliable representations of flow behavior around the bottom intake structure. To achieve the optimum mesh size and demonstrate the independence of simulation results from mesh sizes, five tests were conducted for model T68 with a different mesh size, as shown in Table 7. Comparing the numerical simulation results with the physical model for discharge diverted by the bottom intake (Qd) and the discharge passed over the bottom intake (Qr) revealed significant errors for MITN1 and MITN 2. These mesh sizes were unable to model adequately the void space between the bottom intake bars, resulting in the reduction in diverting flow, and leading to less accurate results. On the other hand, MITN 4 and MITN 5 results were very close to those of MITN 3, indicating that reducing the mesh size had minimal impact on the results. Therefore, by adopting the optimal mesh dimensions according to MITN 3, the desired results can be reliably obtained through numerical simulation, while avoiding the additional cost and time required for modeling with smaller mesh sizes. To illustrate the typical output of the Flow-3D model and provide a visual check of results, the run of the T60 test is shown in Figure (10).

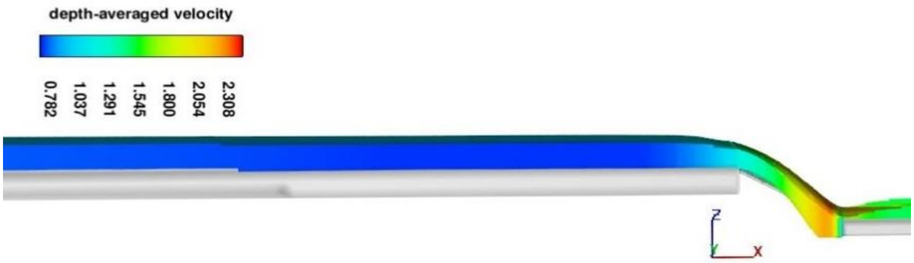

Figure (10): Longitudinal profile of the T60 numerical model by Flow-3D (the X-axis is along the canal and the Z-axis is the elevation axis normal to the canal)

Table 7. Mesh independency test

Mesh Independency Test Number (MITN)	**1**	**2**	**3**	**4**	**5**
Mesh size over the racks (m)	0.006	0.005	0.004	0.003	0.002
E_R(%): Q_d	32.31	17.16	1.19	1.17	1.16
E_R(%): Q_r	-16.90	-7.38	-1.22	-1.15	-1.14

RESULTS AND DISCUSSION

Diverted Discharge Ratio (DDR)

The Diverted Discharge Ratio (DDR), defined as the ratio of diverted discharge to total discharge (Qd/QT), is a crucial dimensionless parameter that indicates the efficiency of bottom intake racks in diverting river flow. To analyze the variations in DDR and the factors influencing it, numerical model results were employed. The DDR values were obtained from models with varying geometric parameters (rack slope S1 and rack length L) and plotted against QT, as shown in Figure (11). The following observations can be made from the Figure (11) diagrams:

1. **Decrease in DDR with Increasing QT**: The DDR decreases as QT increases across all bottom racks, regardless of their geometry. This is attributed to the increase in specific energy of the incoming flow, resulting in a larger volume of water passing over the rack.
2. **Effect of Rack Slope**: The DDR decreases with an increase in the rack slope. This is due to flow separation caused by acceleration over the inclined rack. The decrease in DDR is more pronounced for longer racks.
3. **Effect of Rack Length**: The DDR decreases with a decrease in rack length because shorter racks provide less surface area for the flow to divert through.

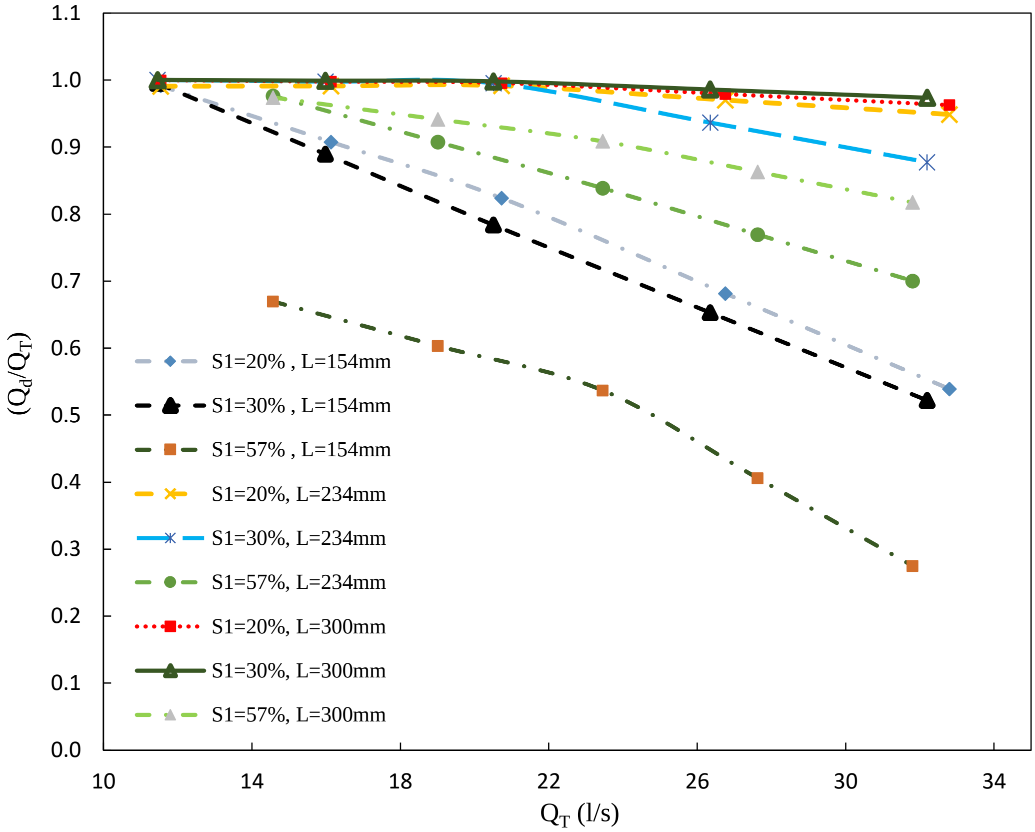

Figure (11): Summary of model results for Qd and Qr and estimation errors

Pressure Distribution

Pressure distribution is a significant factor in the analysis of open channel flows, as it helps in predicting the stress conditions at the solid boundaries accurately. Figure (12) illustrates the pressure contours along the bottom rack for three tests, with results extracted at the 13th second of runtime for the flow centerline. The pressure distribution diagram reveals that the maximum negative pressure occurs in Test T64. This suggests that the maximum negative pressure on the bottom racks is independent of the discharge value, but has a consistent location. The increased negative pressure around the bars enhances the diverted discharge through the bars.

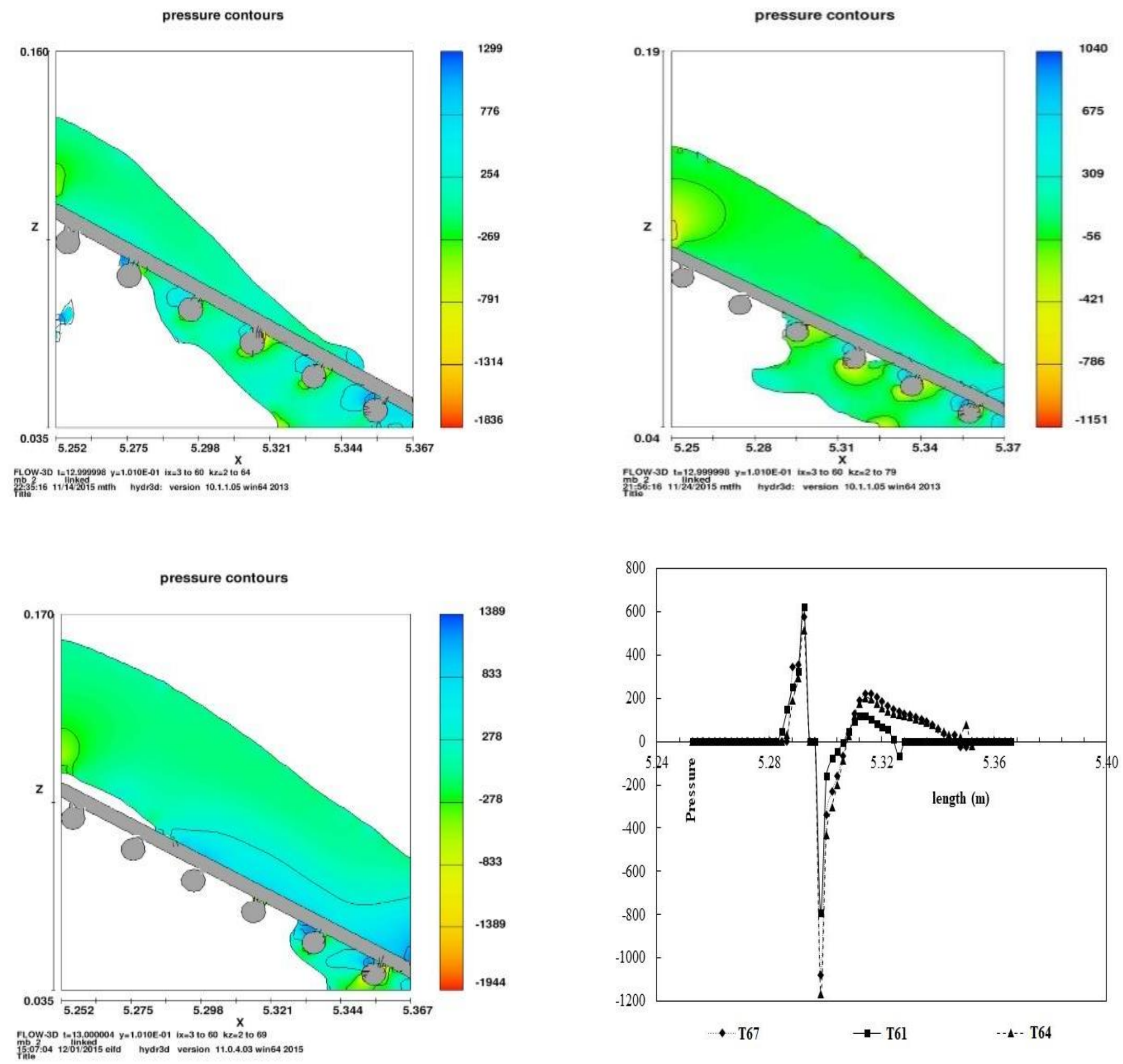

Figure (12): Pressure contour along the bottom rack, a) top left for T61, b) top right for T64, c) bottom left for T67, and d) pressure diagram along the bottom rack for 3 tests

Output Velocity Distribution

The output velocity distribution of fluid particles through the intake bars (z-direction velocity) is shown in Figure (13). The vertical velocity distribution indicates that at the start of the intake, due to the high flow velocity and acceleration, there is no outflow. However, outflow initiates after approximately 30% of the rack length in all three tests. Additionally, higher approach discharge delays the onset of outflow due to increased flow momentum.

Discharge Dividing Streamline (DDS) Position

To determine the diverted discharge using the DDS method for the mesh-panel bottom rack, the deep velocity distribution function in the channel section must be known. Bina (2018) utilized the deep velocity profile proposed by Guo and Julien (2008), which showed good agreement with laboratory results:

$$\frac{V}{U_*} = \frac{1}{\kappa}\ln\left(\frac{U_* y}{\upsilon}\right) + D_1 + \frac{2\Pi}{\kappa}\sin^2\left(\frac{\pi\zeta}{2}\right) - \frac{\zeta}{3\iota} \qquad (7)$$

where V is the velocity at a distance y from the channel bed, U_* is the boundary shear velocity, κ is the von Karman constant (0.4), and ρ, and μ are fluid density and dynamic viscosity, respectively. In the above equation, ζ is the non-dimensional depth of the position of the maximum velocity to the channel bed, which is obtained from the equation $\zeta = y/\delta'$. In the aforementioned equation, δ' is the distance from the location of the maximum velocity to the channel bed, which depends on velocity distribution in the channel section. According to Guo and Julian's research, deep velocity distribution can be considered as a parabolic function ($V = ay^2 + by + c$), where a, b, and c are regression parameters. Thus, the location of the maximum velocity to the channel bed (dip position) is $\delta' = -b/2a$. Bina [2018] proposed the values of D_1 and Π in Equation (7) as 3.314 and 0.011, respectively, by using non-linear regression in a way that had the highest correlation with the experimental data $\left(R^2 = 0.987\right)$.

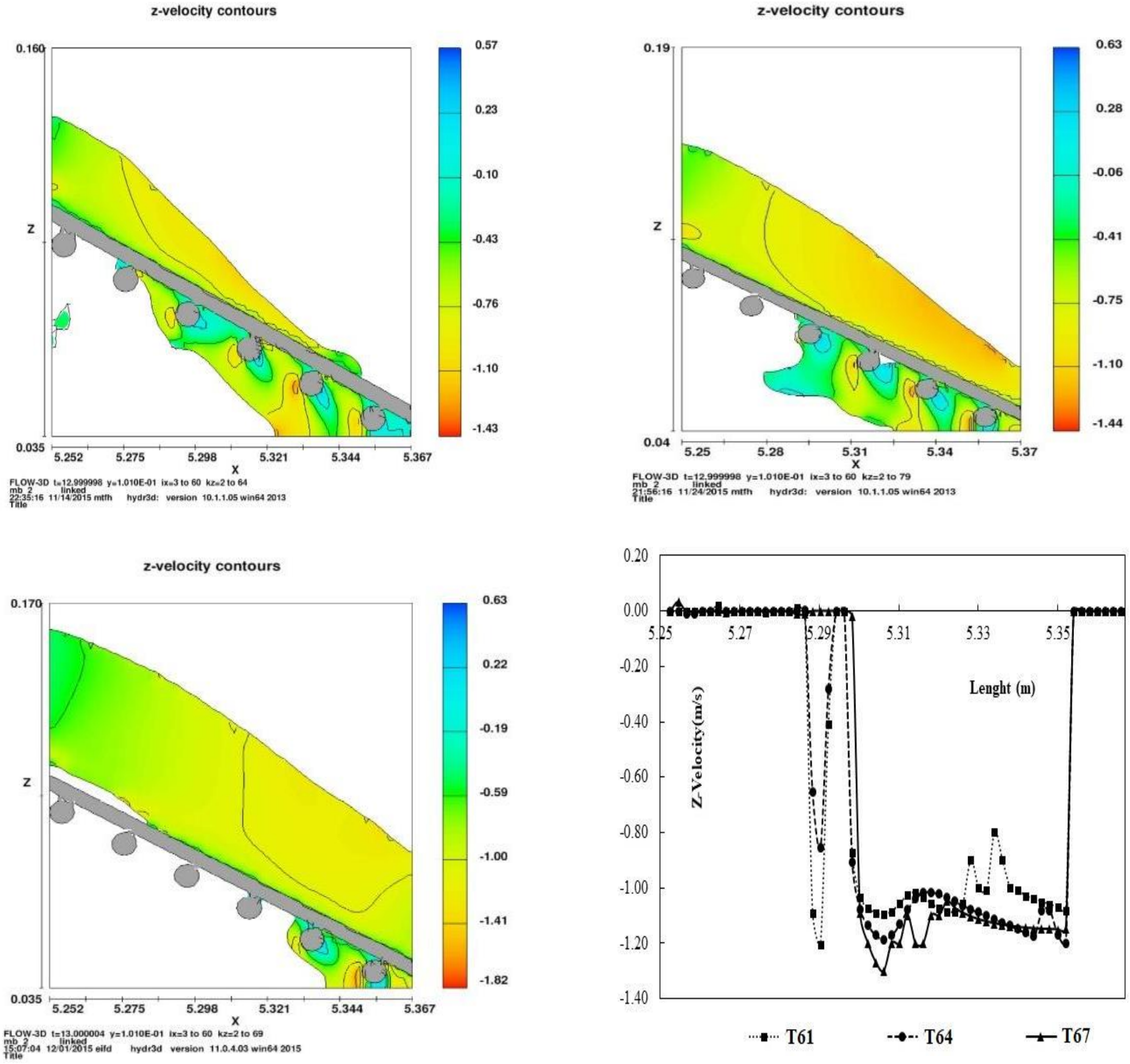

Figure (13): Z-velocity contour along the bottom rack, a) top left for T61, b) top right for T64, c) bottom left for T67, and d) velocity diagram along the bottom rack for 3 tests

Using the numerical model in Flow-3D, this velocity profile was compared with experimental results from Bina (2018). A canal cross-section upstream of the bottom intake was selected to avoid the intake's influence on the velocity profile, and profiles were extracted at three different discharges, showing good agreement Figure (14).

The DDS position was then located using the numerical model data. Figure (15) shows the DDS position in the models for some discharges, and the numerical y′ position was compared with experimental data, yielding a coefficient of determination (R^2=0.98) and a relative error (E_r=0.32%), indicating a good match between numerical and experimental data.

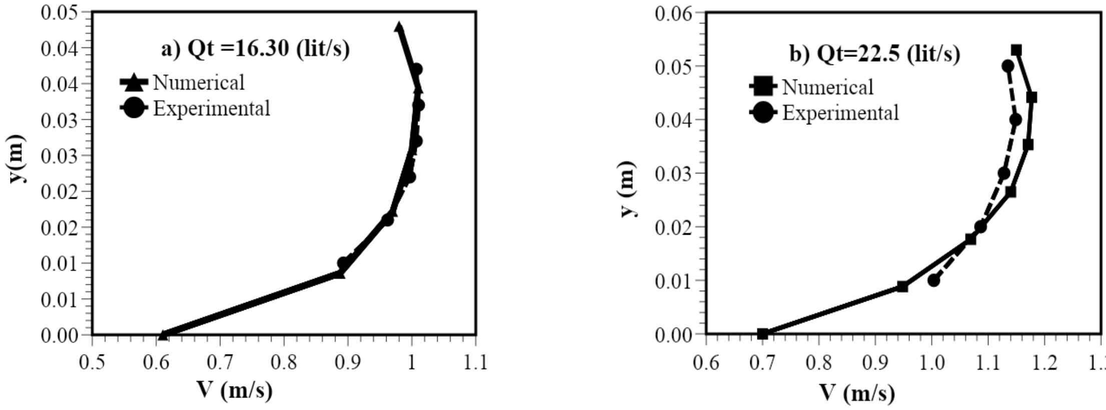

Figure (14): Comparison of numerical and experimental deep velocity profiles for different discharges

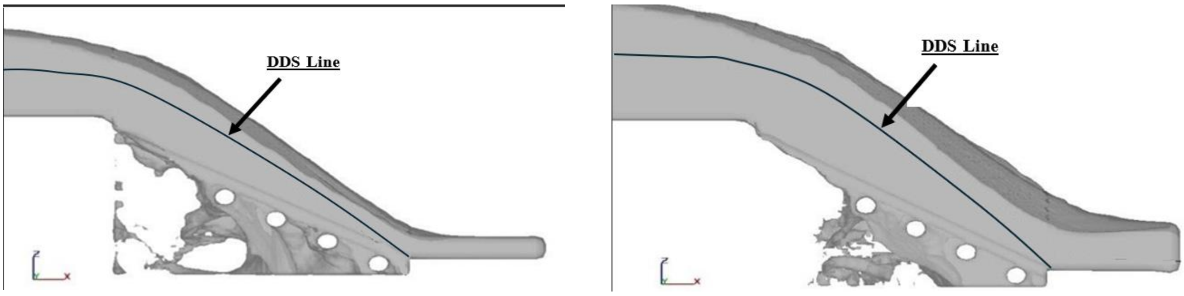

Figure (15): The position of the discharge dividing streamline (DDS) line for a) T64 and b) T67

The DDS line theoretically ends at the downstream edge of the rack, as observed in Figure (1). This was confirmed for test T64; however, for test T67, a 4.2% error in y′ estimation caused the DDS line to extend slightly beyond the rack. The summary of model results for y' is shown in Table 8 and a comparison of numerical and experimental results of the DDS position (y′) is shown in Figure (16).

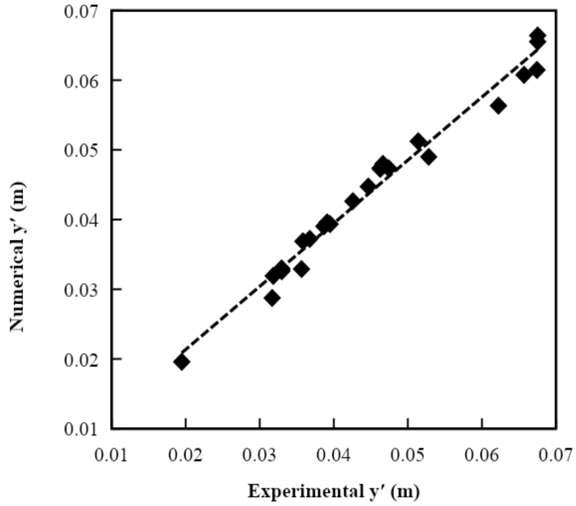

Figure (16): Comparison of numerical and experimental results of the DDS position (y′) in all tests

Based on the numerical model results, a regression equation can be formulated to estimate the normalized DDS position. Using Buckingham Pi theorem and performing linear and non-linear regression on numerical results (with SPSS), the normalized DDS position (y′) for non-sediment flow conditions in an open canal can be expressed as:

$$log\left(\frac{y'}{y_0}\right) = 0.25 + 0.266 log\left(\frac{L}{y_0}\right) - 0.18\, log\, log\,(S_1) - 0.114 lo\, g(Re) \quad (8)$$

This equation was derived from experimental data and thus has certain limitations regarding its applicability, as outlined in Table 1. Key limitations include the super-critical flow state (Fr>1), rack void ratio (ϵ=0.4), and rack installation slope (S1 = 22%-57%). Additionally, the proposed equation assumes non-backwater or submerged conditions in both downstream diversion channels (upper and lower apron).

Table 8. Summary of model results for *y'* and estimation errors

Test No.	Boundary Conditions				Experimental *y'* (mm)	Numerical *y'* (mm)	Error (%)
	Q_T (l/s)	Y_0 (mm)	Q_r (l/s)	Q_d (l/s)			
T60	11.48	33	0.30	11.18	31.60	29.8	5.78
T61	11.53	33	1.22	10.31	29.40	28.3	3.89
T62	11.39	33	0.52	10.87	30.80	30.1	2.32
T63	19.73	47	2.95	16.79	44.50	44	1.27
T64	19.88	47	7.55	12.34	35.80	34.1	4.6
T65	19.69	47	3.90	15.79	37.00	37.7	-1.79
T66	28.16	62	8.60	19.56	40.20	41.1	-2.2
T67	29.12	62	13.77	15.35	32.40	33.7	-4.2
T68	28.27	62	9.42	18.85	38.90	39.4	-1.3
T100	12.45	35	0.12	12.34	35.00	34.7	0.98
T101	12.29	35	0.26	12.04	34.30	34.1	0.67
T102	12.40	35	0.06	12.34	34.90	34.8	0.22
T103	20.89	49	0.96	19.92	48.80	47.3	3.11
T104	20.63	49	4.51	16.12	41.00	40.1	2.29
T105	20.65	49	1.09	19.56	46.10	45.6	1.06
T106	32.55	68	3.70	28.85	57.80	57.1	1.29
T107	31.92	68	13.93	17.98	41.30	39.9	3.33
T108	31.91	68	6.31	25.60	56.10	55.5	1.06
T230	10.45	31	0.00	10.45	30.60	31.4	-2.86
T231	10.37	31	0.06	10.31	30.20	30.7	-1.52
T232	10.45	31	0.00	10.45	30.60	30.9	-1.04
T233	20.29	48	0.73	19.56	45.00	46.2	-2.49
T234	20.35	48	3.90	16.45	41.00	41.7	-1.86
T235	20.05	48	0.84	19.21	46.70	46.1	1.17
T236	32.63	67	2.09	30.54	60.00	61.1	-1.77
T237	31.79	67	11.14	20.65	42.30	42.8	-1.01
T238	31.93	67	4.73	27.21	53.30	54.5	-2.3

CONCLUSIONS

Bottom racks are widely used on mountain-rivers to divert flow for small hydropower projects. This paper investigated the hydraulic behavior of a mesh-panel bottom rack (consisting of longitudinal bars over transverse bars) in clear-water conditions using a numerical model developed with the Flow-3D finite volume code. The study focused on the discharge dividing streamline (DDS), which terminates at the downstream end of the mesh-panel bottom rack. An empirical regression equation for DDS position was derived based on model results. The diverted discharge by the bottom rack served as an index to evaluate the best turbulence model, with the RNG k-ε model showing the best correlation between laboratory data and model results. Mesh-independence tests identified a convenient 4-mm cell size for the intake body region. The numerical model was calibrated and validated against Bina's experimental data, resulting in an average relative error of 3.4% for the estimated diverted discharge (Qd) and 1.9% for the remaining discharge (Qr), with standard deviations of errors at 5.41% and 8.25%, respectively, indicating appropriate coordination between experimental and model results. The study of pressure distribution and vertical flow velocity over the bottom rack revealed that negative pressure around the transverse bars increased the diverted discharge through the bars. The vertical velocity distribution showed that, at the beginning of the intake, there was no output flow due to flow velocity and acceleration. Outflow initiated after approximately 30% of the rack length was passed. The deep velocity distribution extracted from the Flow-3D code was used to locate the DDS position, achieving a coefficient of determination ($R^2 = 0.98$) and a relative error ($E_r = 0.32\%$), demonstrating a good match between the numerical model and experimental data. Consequently, a regression relation was proposed to estimate the normalized position of the DDS using the model results. This method allows for easy determination of diverted discharge by the bottom rack in river diversion projects, simply by measuring the approaching flow depth without the need for complex measurement tools. Although our study demonstrated a good correlation with experimental data and the development of an empirical regression equation, it is essential to address the limitations and uncertainties that may affect the generalizability or reliability of the results. Some of the key limitations in the present study were:

1. Due to limitations in laboratory equipment, measuring devices, and pump power, it was not possible to establish unsteady flow (flood condition), higher flow discharge, depth, and higher Froude numbers. Also, due to the limitations of the laboratory flume dimensions, in all experiments conducted, the incoming flow depth was less than the rack length.
2. Although bottom racks are applied mainly in mountain rivers with steep slopes and supercritical flow condition, and consequently the Froude number of all experiments were considered larger than 1, in some cases and projects, the racks maybe used in rivers with low slopes and sub-critical flow.
3. Due to the limitations of the model dimensions and the unchanging slope of the laboratory flume, the range of changes in the Froude number in the experimental tests of this research was within a small range (1-1.5).
4. Bed load sediment condition was not considered in this article, but it was considered in Bina and Saghi (2017) with the same experimental data and conditions of the present study.
5. Results are tried to be free of scaling effects using model-prototype Froude number similarity.
6. There is a narrow set of experimental data for this specific geometry called “mesh-panel bottom rack” and even no field data. Bina and Saghi (2017) studied this form of bottom rack numerically and experimentally for the first time; so, just their data was available to calibrate and validate the model.

Addressing these limitations will provide a more comprehensive understanding of our study's findings and guide future research efforts to enhance the model's robustness and applicability.

REFERENCES

Andaroodi, M. (2005). “Standardization of civil engineering works of small hydropower plants and development of an optimization tool”. Laboratory of Hydraulic Constructions (LCH), Switzerland.

Anderson, J.D. (1995). “Computational fluid dynamics: The basics with applications”. McGraw-Hill Education.

Bina, K. (2018). “Using dividing discharge streamline concept for estimating diverted discharge in mesh-panel bottom racks”. Flow Measurement and Instrumentation Journal, 61, 38-48. https://doi.org/10.1016/j.flowmeasinst.2018.03.004

Bina, K., and Saghi, H. (2017). “Experimental study of discharge coefficient and trapping ratio in mesh-panel bottom rack for sediment and non-sediment flow and super-critical approaching conditions”. Experimental Thermal and Fluid Science, 88, 171-186. https://doi.org/10.1016/j.expthermflusci.2017.01.005

Bina, K., Rikhtehgarmashhad, S., Hosseini, K., and Karami, H. (2024). “Numerical estimation of discharge coefficient for non-circular bottom intake racks”. Applied Water Science, 14, 103. https://doi.org/10.1007/s13201-024-02164-9

Brunella, S., Hager, W.H., and Minor, H.E. (2003). “Hydraulics of bottom rack intake”. International Journal of Hydraulic Engineering, 129 (1), 2-10.

Castillo, L.G., Carrillo, J.M., and García, J.T. (2013). "Flow and sediment transport through bottom racks, CFD application and verification with experimental measurements". Proceedings of 2013 IAHR Congress, Tsinghua University Press, Beijing, China.

Castillo, L.G., García, J.T., and Carrillo, J.M. (2016). "Experimental and numerical study of bottom rack occlusion by flow with gravel-sized sediment: Application to ephemeral streams in semi-arid regions". Water, 8 (4), 166.

Castillo, L.G., García, J.T., and Carrillo, J.M. (2017). "Influence of rack slope and approaching conditions in bottom intake systems". Water, 9 (1), 65.

Castillo, L., and Delgado, M. (2015). "Numerical modeling of sub-critical flow over bottom racks using VoF method". Journal of Hydraulic Research, 53 (4), 495-508. https://doi.org/10.1080/00221686.2015.1039571

Chanson, H. (2004). "Environmental hydraulics of open channel flows". Elsevier.

Ghasemzadeh, F. (2013). "Simulation of hydraulic issues in Flow-3D". Noavar Publications, Tehran, First Edition (in Persian).

Ferziger, J.H., and Peric, M. (2002). "Computational methods for fluid dynamics". Springer.

Ghaderi, A., Dasineh, M., Abbasi, S., and Abraham, J. (2020). "Investigation of trapezoidal sharp-crested side weir discharge coefficients under sub-critical flow regimes using CFD". Applied Water Science, 10 (1), 31.

Guo, J. (2002). "Hydraulic resistance due to sediment deposition in open channels". Journal of Hydraulic Engineering, 128 (12), 1082-1086. https://doi.org/10.1061/(ASCE)0733-9429(2002)128: 12(1082)

Guo, J., and Julien, P. (1997). "Shear stress in smooth rectangular open-channel flows". Journal of Hydraulic Engineering, 123 (10), 939-947. https://doi.org/10.1061/(ASCE)0733-9429(1997)123:10(939)

Guo, J., and Julien, Y. (2008). "Application of the modified log-wake in open channels". Journal of Applied Fluid Mechanics, 1 (2), 17-23.

Hager, W.H. (2010). "Wastewater hydraulics: Theory and practice". Springer.

Henderson, F.M.N. (1966). "Open channel flow". Mac-Millan, New York.

Hosseini, K., Rikhtegar, Sh., Karami, H., and Bina, K. (2015). "Application of numerical modeling to assess geometry effect of racks on performance of bottom intakes". Arabian Journal of Science and Engineering, 40 (3), 677-684.

Julien, P.Y., and Simons, D.B. (1985). "Sediment transport capacity of overland flow". Transactions of the ASAE, 28 (3), 755-762.

Khodier, M.A., and Tullis, B.P. (2022). "Influence of crest roughness on weir flow conditions for improving Nappe stability". Jordan Journal of Civil Engineering, 16 (4), 681-689.

Khozani, Z.S., Khosravi, K., Torabi, M., Mosavi, A., Rezaei, B., and Rabczuk, T. (2019). "Shear stress distribution prediction in symmetric compound channels using data mining and machine learning models". arXiv preprint arXiv:2001.01558

Kumar, S., Ahmad, Z., Kothyari, U.C., and Mittal, M.K. (2010). "Discharge characteristics of a trench weir". Flow Measurement and Instrumentation Journal, 21, 80-87.

Kuriqi A., Pinheiro A., Sordo-Ward A., Bejarano M., and Garrote L. (2021). "Ecological impacts of run-of-river hydropower plants: Current status and future prospects on the brink of energy transition". Renewable and Sustainable Energy Reviews, 142. https://doi.org/10.1016/j.rser.2021.110833

Novak, P., Moffat, A.I.B., Nalluri, C., and Narayanan, R. (2001). "Hydraulic structures". Taylor & Francis.

Noseda, G. (1956). "Correnti permanenti con portata progressivamente decrescente, defluenti su griglie di fondo". L'Energia Elettrica, 33 (6), 565-581 (in French).

O'Hara, N.P., and Pelletier, J.D. (2007). "Fish passage through culverts in Montana: A performance and design study". Journal of the American Water Resources Association, 4 (6), 1515-1529. doi:10.1111/j.1752-1688.2007.00125.x

Orth, D., McClure, G., and Warner, A. (1954). "Hydraulic characteristics of bottom rack intakes". Hydraulic Engineering Proceedings, 12 (1), 29-37.

Patil, D.B., Sohoni, P., and Jadhav, R.P. (2021). "Evaluation of assorted profiles in bridge pier exposed to exciting flood loading". Jordan Journal of Civil Engineering, 15 (4), 633-649.

Righetti, M., and Lanzoni, S. (2008). "Experimental study of the flow field over bottom intake racks". Journal of Hydraulic Engineering, 134 (1), 15-22.

Saleh, L.A.M., and Khassaf, S.I. (2023). "Effects of chute block geometry on the performance of the USBR II Stilling basin". Jordan Journal of Civil Engineering, 17 (3), 513-523.

Wong, K.C. (2009). "Hydraulics of bottom rack chamber for super-critical flow diversion". M.Phil. Thesis, The University of Hong Kong, Hong Kong, China.

Wong, W. (2010). "Computational fluid dynamics simulation of supercritical flow through bottom racks". Flow-3D Journal, 15 (2), 45-58.

Zerihun, Y.T. (2015). "Numerical simulation of flow in open channels with bottom intake racks". Water Utility Journal, 11, 49-61.